

In situ biosensing of the nanomechanical property and electrochemical spectroscopy of ***Streptococcus mutans***-containing biofilms

This article has been downloaded from IOPscience. Please scroll down to see the full text article.

2013 J. Phys. D: Appl. Phys. 46 275401

(<http://iopscience.iop.org/0022-3727/46/27/275401>)

View [the table of contents for this issue](#), or go to the [journal homepage](#) for more

Download details:

IP Address: 140.116.87.75

The article was downloaded on 19/06/2013 at 03:18

Please note that [terms and conditions apply](#).

In situ biosensing of the nanomechanical property and electrochemical spectroscopy of *Streptococcus mutans*-containing biofilms

Bernard Haochih Liu, Kun-Lin Li, Kai-Li Kang, Wen-Ke Huang and Jiunn-Der Liao

Department of Materials Science and Engineering, National Cheng Kung University, Taiwan, ROC

E-mail: hcliu@mail.ncku.edu.tw and hcliu@alumni.stanford.edu


Received 9 February 2013, in final form 18 April 2013

Published 18 June 2013

Online at stacks.iop.org/JPhysD/46/275401

Abstract

This work presents *in situ* biosensing approaches to study the nanomechanical and electrochemical behaviour of *Streptococcus mutans* biofilms under different cultivation conditions and microenvironments. The surface characteristics and sub-surface electrochemistry of the cell wall of *S. mutans* were measured by atomic force microscopy (AFM) based techniques to monitor the *in situ* biophysical status of biofilms under common anti-pathogenic procedures such as ultraviolet (UV) radiation and alcohol treatment. The AFM nanoindentation suggested a positive correlation between nanomechanical strength and the level of UV radiation of *S. mutans*; scanning impedance spectroscopy of dehydrated biofilms revealed reduced electrical resistance that is distinctive from that of living biofilms, which can be explained by the discharge of cytoplasm after alcohol treatment. Furthermore, the localized elastic moduli of four regions of the biofilm were studied: septum (Z-ring), cell wall, the interconnecting area between two cells and extracellular polymeric substance (EPS) area. The results indicated that cell walls exhibit the highest elastic modulus, followed by Z-ring, interconnect and EPS. Our approach provides an effective alternative for the characterization of the viability of living cells without the use of biochemical labelling tools such as fluorescence dyeing, and does not rely on surface binding or immobilization for detection. These AFM-based techniques can be very promising approaches when the conventional methods fall short.

 Online supplementary data available from stacks.iop.org/JPhysD/46/275401/mmedia

(Some figures may appear in colour only in the online journal)

1. Introduction

1.1. *Streptococcus mutans*

Streptococcus mutans is a major pathogen that causes dental caries [1–3]. The extracellular polymeric substance (EPS) synthesized by *S. mutans* from sucrose forms a biofilm which attaches to the surface of teeth and serves as the colony of bacteria, and it is also commonly known as dental plaque [2]. In addition, the *S. mutans* secretes weak organic acids as

byproducts, which cause a low pH environment in the mouth, and such acidic conditions eventually lead to demineralization of enamel and the formation of cavities [4]. *S. mutans* is categorized as a Gram-positive bacterium; compared with a Gram-negative bacterium, a Gram-positive bacterium has a relatively thick cell, consisting of several peptidoglycan layers, teichoic acid and lipoteichoic acid.

Since the physiological properties of *S. mutans* provide crucial information about biofilm virulence, it is highly desirable to monitor the characteristics of *S. mutans* under

various conditions rapidly and reliably. Conventional biosensing approaches rely on biochemical methods such as fluorescence dyeing and bio-tagging (labelling), which are sometimes not time effective and may influence the microenvironment of the specimen under test; therefore, there is a need for effective biosensing techniques for quick and reliable evaluation of the viability status of biofilms, especially when they are under common anti-pathogenic procedures such as UV exposure and alcohol dehydration treatment. It is, therefore, the goal of this work to apply AFM and its derivative label-free biosensing techniques to the study of a biofilm about its nanomechanical and electrochemical properties under various microenvironments, and to connect these properties to the viability status of biofilms.

1.2. Label-free detection techniques

Conventional biosensing methods for bacteria rely on biochemical identification. These labelling techniques, including enzyme-linked immunosorbent assay (ELISA) [5, 6], polymerase chain reaction (PCR) [7, 8] and DNA probe hybridization [9, 10], are effective in providing quantitative information with high sensitivity. However, the use of labels may interfere with assays, affecting the accuracy of analysis; the samples usually require pre-enrichment treatment, therefore the detection steps are lengthy and the overall process can be time consuming [11]. In addition, labelling techniques are not suitable for the detection of viable but nonculturable forms [12, 13], thus the applications are restricted.

Label-free methods, on the other hand, have become rather attractive especially for their potential in on-site and real-time point-of-care applications. Various optical techniques such as surface plasmon resonance (SPR), waveguide-based immunosensors and whispering-gallery-mode (WGM) sensors are emerging biosensing methods with promising applications [11, 14, 15]. They detect small changes in the reflective index in an evanescent field, or the shift of wavelength in resonance upon an intermolecular binding event. Other non-optical approaches, including electrochemical impedance spectroscopy (EIS) and microcantilever resonance, were also developed for biosensing applications [16, 17]. The former detects the change in impedance spectrum upon attachment of cells or biochemical binding, and the latter relies on the shift of resonant frequency in cantilever vibration due to an antibody immobilization event.

Although without the need of labels, these label-free techniques still require the binding (or adsorption) of the cells or molecules to the sensors. Surface treatment to immobilize the molecules/cells of interest is essential and may influence the accuracy and sensitivity of measurements. In this work, direct measurements of the properties (both nanomechanical and electrochemical) of cells were performed without labelling or surface treatments; the physiological status of cells under test was characterized as the foundation of biosensing in this study.

1.3. AFM-based techniques

In recent years, scanning probe techniques, such as atomic force microscopy (AFM), have been widely used for the study of biomaterials due to their versatile functionality, flexibility in sample condition and excellent nanoscale resolution among other biosensing techniques [18–20]. Previous AFM studies of *S. mutans* focused on the surface morphology and roughness of different strains, or analyses of the tip–cell adhesion force under various sucrose treatment times. Nonetheless, the capability of multiple-property mapping and *in situ* measurements of *S. mutans* have not been well developed and demonstrated.

Nanoindentation is an effective method to measure the mechanical properties of a nanomaterial, such as its elastic modulus [21, 22]. However, commercial nanoindenters face several challenges when it comes to examining biomaterials such as bacteria and cells. For instance, the radius of curvature (ROC) of a nanoindenter tip is typically larger than 100 nm, which restricts the probing of interesting nanoscale features on the surface. In addition, the navigation of a specimen's surface (either by optical microscopes or nanoindenter scanning) is typically laborious, and the resolution is in the micrometre range. Moreover, the force exerted by a nanoindenter is in the order of micro-newton magnitude, which can be too large to probe the delicate features of biomaterials. An alternative characterization approach is nanoindentation using an AFM probe [23, 24]. The high positioning accuracy of AFM makes it possible to select small regions and map the nanomechanical properties individually [25, 26]. With its nanoscale needle-like tip (ROC < 10 nm), AFM is capable of acquiring detailed information in selected nanoscale regions, and resulting in less damage on nanomaterials and biological samples [27].

Most AFM systems are equipped with a force spectroscopy nowadays. In this measurement mode, the AFM probe is able to maintain its lateral position on a selected spot of the sample surface identified by a pre-measurement survey scan. The results are interpreted as force–displacement curves, which record the deflection of the cantilever when the tip is compressing into or withdrawing from the sample. With its great sensitivity with regard to detecting physical interactions between the tip and cell, force spectroscopy provides the opportunity to examine both the cytoskeleton and nanomechanical properties of biological samples.

Electrochemical methods are real-time, non-invasive analytical techniques that have many applications in the inspection and detection of biomaterials [17, 28, 29]. As conventional EIS uses millimetre-sized electrodes that cannot resolve spatial information on the microscale, new techniques with smaller electrodes and advanced measurement setups have been developed. A scanning impedance microscope (SIM) is a technology which combines the functions of EIS and AFM, and with the versatile measurement and precision stage control of an AFM platform, SIM is able to measure a specimen's local impedance responses via a nano-sized AFM probe tip [30–33].

The measurement time for the AFM-based techniques is relatively short when compared with conventional biosensing methods. For a measurement area of $5\ \mu\text{m} \times 5\ \mu\text{m}$, the

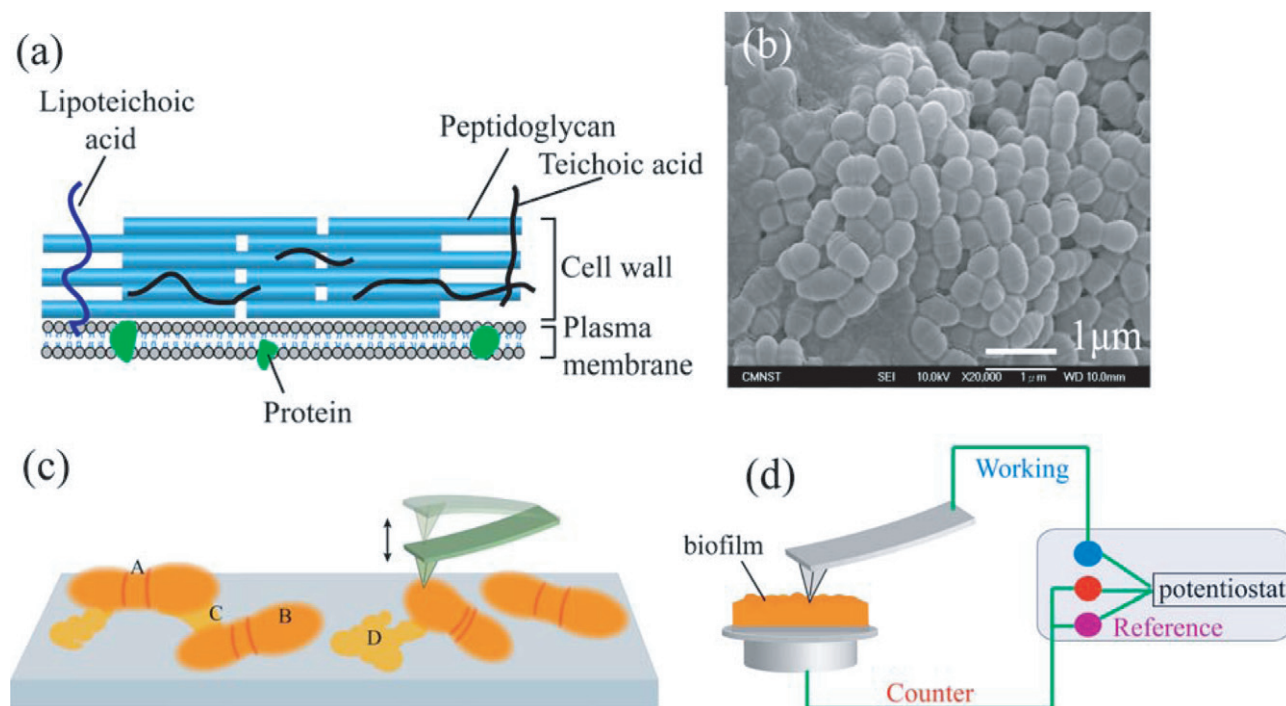


Figure 1. (a) Structure of a Gram-positive bacterial cell wall. The cell wall is composed of peptidoglycan layers, lipoteichoic acid and teichoic acid, with the latter two interspersed perpendicular to peptidoglycan layers. (b) SEM image of a dehydrated *S. mutans*-containing biofilm after 24 h culture. (c) Schematic diagram illustrating the nanoindentation setup with an AFM probe on specific areas: (A) Z-ring (septum), (B) cell wall, (C) interconnecting area between two bacteria, (D) EPS. (d) Schematic diagram for the AFM-based electrochemical spectroscopic measurement setup on the *S. mutans* biofilm.

pre-measurement AFM scan (topography) takes 5–15 min; a nanomechanical measurement (nanoindentation or force-curve) takes 1–2 min, and the SIM measurement for a full frequency spectrum usually takes 15–20 min. Most of the AFM experiments in this work were completed within 30 min. Therefore, the AFM-based techniques (such as AFM nanoindentation and SIM) would be suitable over the fluorescent stain method in cases such as when quick screening is needed, or when photobleaching is a problem.

2. Experimental details

2.1. *Streptococcus mutans* culture

In the experiments, *S. mutans* (ATCC 25175) biofilm was cultured in Brain Heart Infusion (BHI) liquid (Merck, Darmstadt, Germany). High-temperature sterilized glass coverslips with dimensions of 5 mm × 5 mm were used as substrates for cultivation and placed in the wells of a 24-well microplate; a droplet of 5×10^8 colony-forming-unit per millilitre (CFU ml⁻¹) bacteria liquid was applied on each substrate. 1000 μl BHI liquid consisting of 0.15% sucrose (Merck, Darmstadt, Germany) was added to the wells and cultured at 37 °C. The substrates were incubated in an atmosphere of 80% N₂, 10% CO₂ and 10% H₂, and the BHI liquid was changed every 24 h; other details of the biofilm cultivation process are included in a prior study [34]. *S. mutans* specimens with 24 and 48 h cultivation time were prepared based on the above steps. In addition, the preparation of isolated clustered or single *S. mutans* was carried out by placing

a droplet of 5×10^8 CFU ml⁻¹ bacteria liquid on the substrate; the specimen was taken out of the liquid and exposed in air (at room temperature, relative humidity ~60%) before AFM measurements. The porous EPS structure in the biofilm helps to contain the fluid and keep the biofilm surface moist after exposure in air [35]. The dehydrated *S. mutans* was prepared by soaking the cultured substrates in 95% alcohol for 1 h, removing the substrates from the alcohol bath, and then leaving the substrates exposed in an ambient environment before AFM measurements. The morphological identifications of *S. mutans* and the measurement setup are described in figure 1.

For the experiments on ultraviolet (UV) radiation, a UV-C253.7nm lamp (TUV36W, Philips, the Netherlands) was used. The nominal wavelength of the light source is 253.7 nm (UV-C) with a power of 36 W, and the *S. mutans*-containing biofilms were kept under wet conditions during exposure. The lamp–specimen distance was kept at 50 cm during the exposure. Based on our preliminary study, the wet condition was provided by spreading mists of sanitized, deionized water every 30 s on the surface of the biofilms to prevent temperature rise and drying of the specimen by UV exposure.

2.2. Viability check

In order to confirm that the *S. mutans* cell was still alive after biomechanical measurement, we used a fluorescence microscope (DMIRB, Leica, Germany) and the live/dead BacLight Bacterial Viability Kit (Molecular Probe Inc., Eugene, OR, USA) to observe the viability of the cell after AFM nanoindentation. The Viability Kit consists of

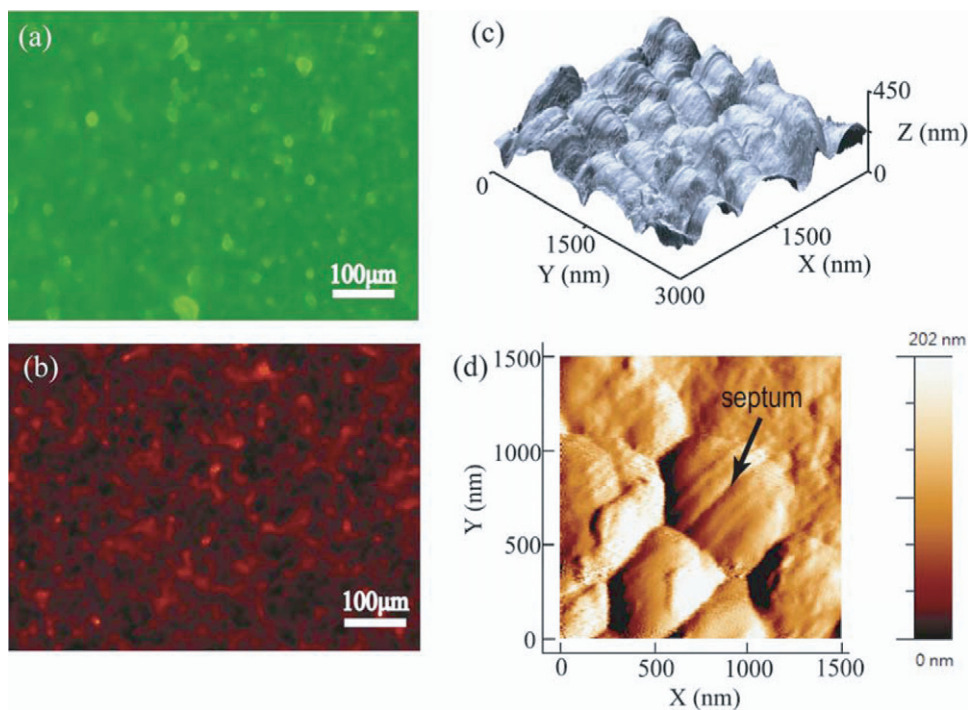


Figure 2. Fluorescent and AFM topography images of the *S. mutans*-containing biofilm. (a) Fluorescent image of the biofilm after AFM nanoindentation; the green dye indicates that most of the *S. mutans* were still alive; (b) fluorescent image of the biofilm after dehydration; the red dye indicates that most of the *S. mutans* were dead; (c) AFM 3D image of the alive *S. mutans*-containing biofilm, which represents its surface morphology; (d) AFM 2D image showing the detailed septum (Z-ring) area of the alive *S. mutans* biofilm.

two nucleic acid stains, propidium iodide (PI) and green-fluorescent nucleic acid stains (SYTO 9), showing green (alive) or red (dead) colour under FM for easy identification of the viability of the *S. mutans* biofilm (figures 2(a) and (b)).

In our preliminary study ($n = 4$, 95 % confidence level) of the *S. mutans* biofilm, in which the viability was checked with a fluorescent dye, more than 90% *S. mutans* were still alive after 30 min of exposure in air, and about 70% were still alive after 1 h of exposure.

2.3. AFM/SPM methodology

After the *S. mutans* biofilms were freshly prepared, the specimens were quickly taken out of the liquid and allowed to dry while exposing in air; they were then transferred to an AFM system (BASO AFM, Force Precision Instrument, Co., Taiwan) for inspection within an hour. Topographic AFM scan images in 2D and 3D (figures 2(c) and (d)) were acquired in tapping scan mode (intermittent contact) in air, by a single crystal silicon probe with a typical spring constant of $0.25\text{--}0.3\text{ N m}^{-1}$ and tip ROC less than 10 nm (ContA1, Budget Sensors, Bulgaria).

The AFM nanoindentation experiments were carried out using the following procedures. First, the biofilm specimen surface was wide-scanned to obtain a topographical image to map out the specific locations of the biofilm, and then quantitative measurements of the local biomechanical properties of selected locations on the *S. mutans*-containing biofilm using AFM force spectroscopy were made. The elastic moduli and cell metabolism of *S. mutans* with different cultivation times were analysed on the following four locations:

Z-ring (septum), cell wall, the interconnecting region between two bacteria and EPS (figure 1(c)). Since the cell wall represents the most accessible surface feature with the highest coverage among the four locations, we chose the cell wall as the measurement site for electrochemical spectroscopy and UV exposure study.

In order to acquire the electrical properties of the *S. mutans*-containing biofilm, an Au-coated conductive AFM probe (PPP-ContAu, Nanosensors, Neuchâtel, Switzerland) was used as a conducting electrode. An aluminum substrate was used as the bottom electrode, and a biofilm was cultivated on the aluminum substrate for impedance measurement by the AFM probe tip (figure 1(d)). The aluminum substrate was chosen among other conductive substrates based on its relative easiness in *S. mutans* cultivation and sufficient electrical conductivity for impedance measurements. The impedance spectra of the *S. mutans*-containing biofilm samples cultured for 24 h with/without dehydration treatment were obtained on a customized AFM system (BASO AFM, Force Precision Instrument, Co., Taiwan). The applied current was 10^{-7} A, and the testing frequency range was set at 300–3000 Hz (Series G 750, Gamry Instruments Inc., USA) (see the figure in online supplementary material (stacks.iop.org/JPhysD/46/275401/mmedia)).

2.4. Statistics

The measurement data collected from six different biofilm statuses and four different regions were processed with the paired student's *t* test at a 95% confidence level; the sample size was $n = 10$ for each biofilm status.

3. Results and discussion

3.1. *In situ* nanomechanical properties

To quantitatively assess the elastic moduli of the Z-ring, cell wall, interconnect and EPS, the force–displacement curves obtained from AFM nanoindentation were analysed using the Hertz model [26]:

$$F_C = \frac{2}{\pi} \tan \alpha \frac{E}{1 - \nu^2} \delta^2 \quad (1)$$

where F_C is the indentation force, α is the half-opening angle of the AFM tip (assumed to be conical), E is the elastic modulus of the specimen, ν is Poisson’s ratio (typically assumed to be $\nu = 0.5$ for a biological specimen) and δ is the indentation depth of the specimen.

The indentation depth of soft *S. mutans* was calibrated by carrying out a force–displacement measurement on a hard reference sample (such as Si_3N_4); the contribution of displacement from the cantilever alone can be obtained by this reference measurement. The correct indentation depth of the specimen was extracted by the following equation:

$$\delta = z - d \quad (2)$$

where z is the total displacement caused by both cantilever deflection and sample deformation, and d is the deflection of the AFM cantilever (more detail about the calibration of the spring constant of the cantilever is provided in the supplementary data stacks.iop.org/JPhysD/46/275401/mmedia). Figure 3 summarizes the elastic moduli of the selected biofilm location under different *S. mutans* conditions (cultivation time and viability). Here, the alive cells are labelled as A and dehydrated ones as D; the single (isolated) *S. mutans* and the growth time are presented by S and 24/48, respectively. The results reveal that the cell wall has the highest elastic modulus, followed by the Z-ring, interconnect and EPS. The differences in elastic moduli are most likely due to variances in the membrane structure and composition. Generally speaking, the exterior structure of both the Z-ring and the cell wall are peptidoglycan, but the stiffness of the Z-ring region is $\sim 75\%$ less than that of the cell wall; since the Z-ring (septum) is where the cell division occurs, our results suggest that the newly formed cell wall in the septum region is structurally less dense during cell division. Furthermore, since Touhami *et al* observed a depression on the newly formed cell wall and suggested the occurrence of peptidoglycan hydrolysis on the septum during cell division [36], we therefore believe that such a hydrolysis reaction reduces the strength of the outer structure of the septum, leading to a lower elastic modulus.

Figure 3 also indicates that the elastic moduli increase with increasing growth time, as well as after the dehydration treatment, due to a stiffened cell wall. It is generally accepted that the top layer of the biofilm should contain freshly grown *S. mutans*; in other words, the elastic modulus of the top surface of the *S. mutans*-containing biofilm should be similar regardless of its growth time. However, *in situ* nanomechanical results suggest otherwise. A possible explanation for this is that some mutations of *S. mutans* with a longer culture

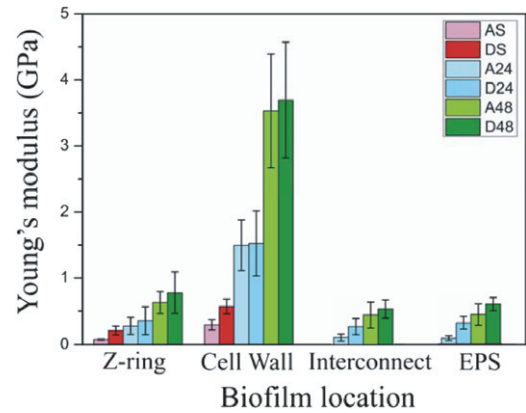


Figure 3. Column plot of the elastic moduli at selected biofilm locations, as shown, under different specimens (AS = alive single, DS = dead single, A24 = alive culture 24 h, D24 = dead culture for 24 h, etc).

time result in an increase in the elastic modulus, but further investigations are needed to confirm this viewpoint.

On the other hand, the elastic moduli of the EPS region and those of the interconnecting region between two cells were very similar, suggesting that the chemical composition and molecular structure of these regions might also be alike. After the dehydration treatment with alcohol, the *S. mutans* became stiffer, and the elastic moduli of the dehydrated specimen increased variously at different locations. On average, the elastic moduli at the Z-ring increased 28% for the 24 h-cultured biofilm, and 24% for the 48 h-cultured ones; the increases at the cell wall for both 24 and 48 h biofilms were insignificant (2–5%). The difference in biofilm cultivation time can also be seen at the interconnect and EPS regions: for 24 h specimens, the increase in elastic moduli after dehydration was 145% at the interconnect and 246% in the EPS region, while the increase in elastic moduli for 48 h biofilms was 20% at the interconnect and 35% at the EPS. For single/isolated cells, the effect of dehydration was more obvious than that of the biofilms; the increase in elastic moduli was 174% at the Z-ring, and 90% at the cell wall.

The deviations of the elastic moduli data came from the individual differences of viability among *S. mutans* cells, as also revealed by the fluorescent dyeing check. Another source of deviations was the diversity in different sample batches. However, in the same specimen, the measured elastic moduli at various locations were distinct—the modulus was the highest in the cell wall, followed by the Z-ring, EPS and interconnect.

The question then arises as to whether one can distinguish between live and dead cells using this method. The answer is yes, but a collective comparison of measurements at several locations has to be made. For example, our data suggested that the increase in elastic moduli after the alcohol treatment is large ($>20\%$) at the Z-ring, interconnect and EPS, thus the comparison of data at all three locations is needed for a reliable viability check. On the other hand, since the cell walls of the biofilms are insensitive to alcohol dehydration (with the exception of single cells), the comparison of moduli at cell walls cannot be used as the alive/dead criterion. Note that our

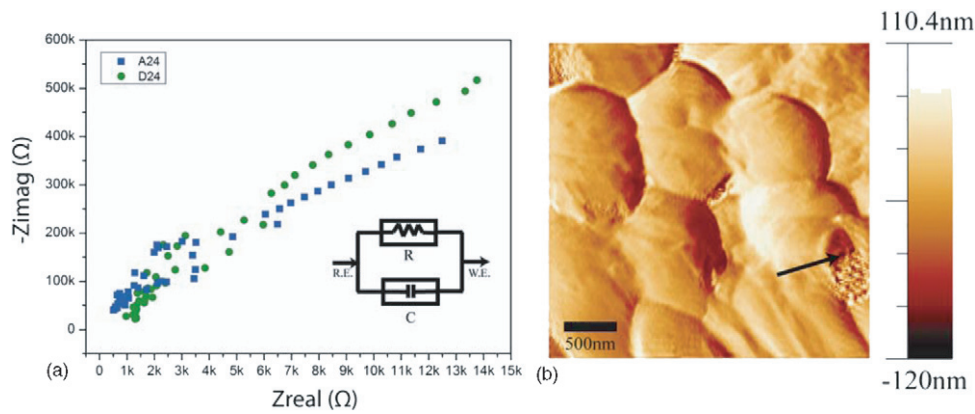


Figure 4. Impedance response of the *S. mutans*-containing biofilm. (a) Nyquist plot and equivalent circuit model of the *S. mutans*-containing biofilm before and after dehydration. (b) AFM image showing the ruptures (indicated by arrow) of the *S. mutans* cell after dehydration.

results also suggested that an overall measurement of elastic moduli by either AFM or nanoindenter, without identification of the locations under test, may not provide meaningful data for viability analysis.

3.2. Electrical properties of *S. mutans*

The Nyquist plot in figure 4(a) shows the impedance spectra measured at the cell wall location of the *S. mutans*-containing biofilm before and after the dehydration treatment by alcohol. To further investigate the differences between these states, the data were analysed by an equivalent circuit model consisting of a resistor and a capacitor in parallel. This model is a reduced equivalent circuit of Fricke’s cellular model after performing some simplifications based on our experimental results [37–40]. The curve-fitted values ($n = 6$) are as follows:

- (1) Alive cells: $R_A = 9.194 \pm 0.814 \times 10^6 \Omega$, $C_A = 1.329 \pm 0.128 \times 10^{-9} \text{ F}$;
- (2) Dehydrated cells: $R_D = 5.146 \pm 0.413 \times 10^6 \Omega$, $C_D = 1.788 \pm 0.121 \times 10^{-9} \text{ F}$.

The result indicates that the resistance of the biofilm decreased and the capacitance behaviour became more prominent after the *S. mutans* containing biofilm was dehydrated. The reduced resistance suggests that there were some conductive substances (such as cytoplasm) surrounding the *S. mutans* after dehydration. Figure 4(b) shows an AFM image of ruptures on dehydrated *S. mutans* cells after a careful inspection on the biofilm surface. It is possible that such ruptures allowed the discharge of cytoplasm, and hence increased the conductivity of the biofilm. In addition, the removal of cytoplasmic liquids also caused shrinking of the cytoskeleton, leading to a smaller separation between lipid layers and more interfaces with capacitive characteristics, hence increased capacitance. Note that the decrease in resistance is about 46% for the dehydrated biofilm compared with the alive one, suggesting that the impedance spectroscopy provides a promising, quick and easy method to check the viability of biosamples.

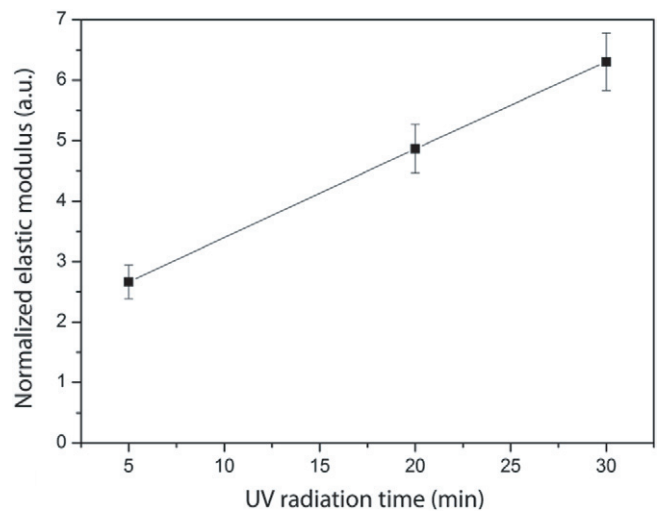


Figure 5. Relation of elastic modulus and UV exposure time for the alive *S. mutans*-containing biofilm. The UV light source has a wavelength of 253.7 nm (UV-C) with a power of 36 W.

3.3. Nanomechanical properties of UV-irradiated *S. mutans*

Based on the above results on the dehydrated and alive *S. mutans*, nanomechanical measurements using AFM were applied on the UV-254 nm irradiated samples prepared under wet conditions. UV light exposure is a common method to disinfect bacteria in drinking water and the medical environment; it has proven to be effective in the reduction of pathogenic microorganisms without producing regulated byproducts. Unlike the disinfection mechanisms of commonly used chemicals such as chlorine and ozone, UV light does not damage cellular structures but the nucleic acid. Since nucleic acid is responsible for metabolic and reproduction functions of all life forms, the UV light inactivates the nucleic acid and prevents the bacteria from replicating [41]. Figure 5 shows that the normalized Young’s modulus of living *S. mutans* surface increased with the UV radiation time. The normalization was performed by setting a reference specimen (non-UV-irradiated) in each group of measurements as 1, and the measurements were divided by this base value accordingly. Since UV exposure does not change the shape and structure of cells, this increase in nanomechanical strength can be

correlated with the viability of *S. mutans*, and possibly a quick and easy method to distinguish *S. mutans*-containing biofilms with different levels of UV radiation.

4. Conclusion

In this work, AFM-based label-free biosensing techniques were introduced to characterize the surface nanomechanical properties and sub-surface electrochemical responses of *S. mutans* biofilms under different anti-pathogenic treatments. For UV radiation treatment of *S. mutans*, AFM nanoindentation revealed a correlation between elastic modulus and UV exposure time; such a correlation provides a method to access the UV radiation damage of cells. The electrochemical measurements revealed that the resistance of the biofilm decreased significantly after dehydration, which suggests the existence of some conductive substances, and the AFM surface morphology image confirmed the presence of ruptures, supporting our assumption of cytoplasm discharge.

We also report on the elastic moduli at various locations of the *S. mutans*-containing biofilm with different statuses. The cell wall exhibited the highest elastic modulus, followed by the Z-ring, EPS and the interconnect area between two bacteria. The dehydrated biofilm had a higher elastic modulus probably due to its stiffer nanostructures. Contrary to expectations, our data also indicate that the elastic moduli of the top surface of the biofilms are higher with a longer cultivation time.

With the *in situ* investigation of *S. mutans* by AFM carried out in this work, we have demonstrated that the AFM nanoindentation and SIM techniques can provide insights into the nanostructures, biomechanical and electrochemical properties of biofilm materials. Biological applications of this approach are very promising and applicable to many other soft biomaterials.

Acknowledgment

The authors are grateful to the National Science Council of Taiwan for the financial support of this work under the contract number NSC 101-2221-E-006-100-MY3.

References

- [1] Loesche W J 1986 Role of *Streptococcus mutans* in human dental decay *Microbiol. Rev.* **50** 353–80
- [2] Hamada S and Slade H D 1980 Biology, immunology, and cariogenicity of *Streptococcus mutans* *Microbiol. Rev.* **44** 331–84
- [3] Kuramitsu H K 1993 Virulence factors of mutans streptococci: role of molecular genetics *Crit. Rev. Oral Biol. Med.* **4** 159–76
- [4] Selwitz R H, Ismail A I and Pitts N B 2007 Dental caries *Lancet* **369** 51–9
- [5] Russell H, Sampson J S, Schmid G P, Wilkinson H W and Plikaytis B 1984 Enzyme-linked immunosorbent assay and indirect immunofluorescence assay for Lyme disease *J. Infect. Dis.* **149** 465–70
- [6] Clark M F and Adams A N 1977 Characteristics of the microplate method of enzyme-linked immunosorbent assay for the detection of plant viruses *J. Gen. Virol.* **34** 475–83
- [7] Blackstone G M, Nordstrom J L, Bowen M D, Meyer R F, Imbro P and DePaola A 2007 Use of a real time PCR assay for detection of the *ctxA* gene of *Vibrio cholerae* in an environmental survey of Mobile Bay *J. Microbiol. Methods* **68** 254–9
- [8] Martinez-Govea A, Ambrosio J, Gutiérrez-Cogco L and Flisser A 2001 Identification and strain differentiation of *Vibrio cholerae* by using polyclonal antibodies against outer membrane proteins *Clin. Diagn. Lab. Immunol.* **8** 768–71
- [9] Wright A C, Guo Y, Johnson J A, Nataro J P and Morris J G 1992 Development and testing of a nonradioactive DNA oligonucleotide probe that is specific for *Vibrio cholerae* cholera toxin *J. Clin. Microbiol.* **30** 2302–6
- [10] Shalon D, Smith S J and Brown P O 1996 A DNA microarray system for analyzing complex DNA samples using two-color fluorescent probe hybridization *Genome Res.* **6** 639–45
- [11] Vollmer F and Arnold S 2008 Whispering-gallery-mode biosensing: label-free detection down to single molecules *Nature Methods* **5** 591–6
- [12] Baker R M, Singleton F L and Hood M A 1983 Effects of nutrient deprivation on *Vibrio cholerae* *Appl. Environ. Microbiol.* **46** 930–40
- [13] Colwell R R 2000 Viable but nonculturable bacteria: a survival strategy *J. Infect. Chemother.* **6** 121–5
- [14] Horváth R, Pedersen H C, Skivesen N, Selmeczi D and Larsen N B 2003 Optical waveguide sensor for on-line monitoring of bacteria *Opt. Lett.* **28** 1233–5
- [15] Oh B-K, Kim Y-K, Park K W, Lee W H and Choi J-W 2004 Surface plasmon resonance immunosensor for the detection of *Salmonella typhimurium* *Biosensors Bioelectron.* **19** 1497–504
- [16] Sungkanak U, Sappat A, Wisitsoraat A, Promptmas C and Tuantranont A 2010 Ultrasensitive detection of *Vibrio cholerae* O1 using microcantilever-based biosensor with dynamic force microscopy *Biosensors Bioelectron.* **26** 784–9
- [17] Maalouf R *et al* 2007 Label-free detection of bacteria by electrochemical impedance spectroscopy: comparison to surface plasmon resonance *Anal. Chem.* **79** 4879–86
- [18] Cross S E *et al* 2007 Nanomechanical properties of glucans and associated cell-surface adhesion of *Streptococcus mutans* probed by atomic force microscopy under *in situ* conditions *Microbiology* **153** (Part 9) 3124–32
- [19] Cross S E, Jin Y-S, Rao J and Gimzewski J K 2007 Nanomechanical analysis of cells from cancer patients *Nature Nanotechnol.* **2** 780–3
- [20] Cross S E *et al* 2006 Atomic force microscopy study of the structure–function relationships of the biofilm-forming bacterium *Streptococcus mutans* *Nanotechnology* **17** S1–7
- [21] Geerligs M, van Breemen L, Peters G, Ackermans P, Baaijens F and Oomens C 2011 *In vitro* indentation to determine the mechanical properties of epidermis *J. Biomech.* **44** 1176–81
- [22] Li C, Pruitt L A and King K B 2006 Nanoindentation differentiates tissue-scale functional properties of native articular cartilage *J. Biomed. Mater. Res. A* **78** 729–38
- [23] Lu L, Oswald S J, Ngu H and Yin F C 2008 Mechanical properties of actin stress fibers in living cells *Biophys. J.* **95** 6060–71
- [24] Notbohm J, Poon B and Ravichandran G 2012 Analysis of nanoindentation of soft materials with an atomic force microscope *J. Mater. Res.* **27** 229–37
- [25] Alsteens D, Dupres V, Mc Evoy K, Wildling L, Gruber H J and Dufrene Y F 2008 Structure, cell wall elasticity and polysaccharide properties of living yeast cells, as probed by AFM *Nanotechnology* **19** 384005

- [26] Touhami A, Nysten B and Dufrene Y F 2003 Nanoscale mapping of the elasticity of microbial cells by atomic force microscopy *Langmuir* **19** 4539–43
- [27] Liu B H and Chang D-B 2011 Simulation-aided design and fabrication of nanoprobes for scanning probe microscopy *Ultramicroscopy* **111** 337–41
- [28] Patolsky F, Zayats M, Katz E and Willner I 1999 Precipitation of an insoluble product on enzyme monolayer electrodes for biosensor applications: characterization by Faradaic impedance spectroscopy, cyclic voltammetry, and microgravimetric quartz crystal microbalance analyses *Anal. Chem.* **71** 3171–80
- [29] Ruan C M, Yang L J and Li Y B 2002 Immunobiosensor chips for detection of *Escherichia coli* O157 : H7 using electrochemical impedance spectroscopy *Anal. Chem.* **74** 4814–20
- [30] Shao R, Kalinin S V and Bonnell D A 2003 Local impedance imaging and spectroscopy of polycrystalline ZnO using contact atomic force microscopy *Appl. Phys. Lett.* **82** 1869–71
- [31] O'Hayre R, Feng G, Nix W D and Prinz F B 2004 Quantitative impedance measurement using atomic force microscopy *J. Appl. Phys.* **96** 3540–9
- [32] Liu B H, Su P-J, Lee C-H and Huang J-L 2013 Linking microstructure evolution and impedance behaviors in spark plasma sintered Si₃N₄/TiC and Si₃N₄/TiN ceramic nanocomposites *Ceram. Int.* **39** 4205–12
- [33] Lee A C, Su P-J and Liu B H 2013 Probing the conductance and microstructure heterogeneity of Si₃N₄/TiC-based nanocomposite at the nanoscale by scanning impedance microscopy *J. Am. Ceram. Soc.* doi:10.1111/jace.12282
- [34] Sladek R E J, Filoche S K, Sissons C H and Stoffels E 2007 Treatment of *Streptococcus mutans* biofilms with a nonthermal atmospheric plasma *Lett. Appl. Microbiol.* **45** 318–23
- [35] Huang W-K, Weng C-C, Liao J-D, Wang Y-C and Chuang S-F 2013 Capillary-tube-based micro-plasma system for disinfecting dental biofilm *Int. J. Radiat. Biol.* **89** 364–70
- [36] Touhami A, Jericho M H and Beveridge T J 2004 Atomic force microscopy of cell growth and division in *Staphylococcus aureus* *J. Bacteriol.* **186** 3286–95
- [37] Ivorra A 2003 *Bioimpedance Monitoring for Physicians: An Overview* Centre Nacional de Microelectrónica Biomedical Applications Group
- [38] Margo C, Prado J, Kouider M, Rouane A and Nadi M (ed) 2006 Bioimpedance spectroscopy for cell characterization in the 50 Hz–5 MHz frequency range *Research in Microelectronics and Electronics* (Piscataway, NJ: IEEE) pp 441–4
- [39] Schulte M B, Dong Z, Tung S, Kim J-W, Wejinya U, Moon H-M and Kong B-W (ed) 2009 Impedance spectroscopy of chicken infectious Laryngotracheitis virus based on atomic force microscopy 2009 *IEEE Int. Conf. on Nano/Molecular Medicine and Engineering (NANOMED) (Tainan, Taiwan)* (Piscataway, NJ: IEEE) pp 249–52
- [40] Franks W, Schenker I, Schmutz P and Hierlemann A 2005 Impedance characterization and modeling of electrodes for biomedical applications *IEEE Trans. Biomed. Eng.* **52** 1295–302
- [41] Snowball M R and Hornsey I S 1988 Purification of water supplies using ultraviolet light *Developments in Food Microbiology* ed R K Robinson and U K Barking (London: Elsevier) pp 171–91